TECHNICAL ARTICLE

Microstructure and Mechanical Properties of AlSi10Mg Parts Produced by the Laser Beam Additive Manufacturing (AM) Technology

Idan Rosenthal · Adin Stern · Nachum Frage

Abstract Selective laser melting (SLM) is an additive manufacturing (AM) technique for fabrication of near net-shaped parts directly from computer-aided design data from a series of layers each one melted on top of the previous one by a laser beam. AlSi10Mg specimens were produced by the SLM technique from gas atomized pre-alloyed powders. The study shows the distinctive layered macrostructure, and the extremely fine cellular dendritic microstructure obtained by the SLM AM process, along with the remarkable tensile testing results for AlSi10Mg components. High thermal gradients determine the small grain sizes of the microstructure. Electron microscopy revealed anisotropy of the parts, inherent to the AM-SLM process, dependent on the build orientation. A ductile, dimpled failure mode was observed in these specimens as expected for a relatively ductile microstructure. It is shown that AlSi10Mg parts produced by SLM display room temperature mechanical properties comparable or even exceeding to those of conventionally cast AlSi10Mg.

Keywords Additive manufacturing · Al alloy · Selective laser melting · Mechanical properties

Introduction

Additive manufacturing (AM) is an appropriate approach for low volume production of geometrically complex lightweight structures. A limited number of investigations on AM of Al-based alloys by selective laser melting (SLM) have been reported [1–3]. There are some difficulties in the successful AM by SLM of Al-based powders. First, the excellent thermal conductivity and high reflectivity (91%) of Al significantly increase the laser power required for melting and secondly, the oxidation of the alloys leads to entrapped oxide inclusions, which create weak spots within the components. The AM technique is a layer-by-layer manufacturing process. A single layer of metal is "deposited" upon a previous layer resulting in complex, time-dependent temperature profiles within the part being fabricated. The exposure period of the laser irradiation is in the range of milliseconds, and the process can be considered as high power density—short interaction time [4]. The microstructure of the as-built aluminum AM-SLM parts is reported to be a very fine cellular–dendrite solidification structure [2]. The formation of this fine dendritic structure upon laser treatment was previously observed in various laser processing techniques, such as laser surface remelting and laser deposition [5]. It was found by Dinda et al. that the high-energy density of the laser along with a directional heat transfer leads to a directional solidification [5]. Moreover, by repeating the deposition of the beads layer after layer, a [100] fiber or cube texture depending on the scanning direction is formed. It has to be pointed out that very high heat inputs during laser deposition process results in a width of a deposited layer of about 1 mm, while a width of a track typically formed in AM-SLM is only 100 μm. In this paper, we describe the unique macro- and microstructural architectures and tensile properties of AM-SLM processed AlSi10Mg alloy.

Experimental

SLM System and the Building Process

The machine for AM is equipped with a 400 W Nd-YAG laser, and a scanning velocity of about 1 m/s was applied.

I. Rosenthal (✉) · A. Stern · N. Frage
Materials Engineering Department, Ben-Gurion University of the Negev, P.O Box 653, 8410501 Beersheba, Israel
e-mail: idanros@bgu.ac.il

Particle size of the AlSi10Mg alloy powder was in the range of 25–50 μm. The starting AlSi10Mg powder was characterized by x-ray diffraction (XRD). Tensile specimens were built in two different directions (vertically and horizontally) and underwent machining with surface roughness and tolerances in accordance with the ASTM E-8 (round specimen, spec 3) standard. The specimens were manufactured using a technique referred to as strip scanning with a continuous change of the scanning direction between each successive layer. The specimens were divided to 8-mm-wide stripes, which were scanned back and forth. Throughout the scans, there were overlapping areas, resulting in remelting of previously melted and solidified regions. Density of the samples was about 2.63 g/cm^3. All the built parts underwent a stress-relieving heat treatment at 300 °C for 2 h.

Optical and Electron Microscopy (OM and SEM)

The macro- and microstructure of the specimens were characterized by optical and scanning electron microscopy (SEM), equipped with an energy-dispersive spectrometer. The specimens were prepared by conventional metallographic methods, with a fine 0.5 μm diamond polish and etched using Flick's reagent (90% H_2O, 10% HF).

Mechanical Properties

Tensile tests were conducted using a universal testing machine. A series of six specimens with two differing build directions were tested, and the stress–strain curves were analyzed. Microhardness tests were conducted using a microhardness tester with 100gf load. The fracture surface was observed in order to clarify the failure mode and its correlation with the microstructure.

Results and Discussion

Alloy Microstructure

Solidification and phase transformations of Al–Si alloys occur according to the Al–Si phase diagram (Fig. 1), with a eutectic composition of about 11–12 wt% of Si. The alloy used in this work is close to the eutectic point, and a lamellar microstructure is expected after solidification and cooling. Actually, this kind of the microstructure is commonly observed in Al–Si cast alloys with similar Si contents (Fig. 2).

The SLM process of adding material track after track and layer after layer together with the fast and directional cooling rates creates a unique macrostructure in the components (Fig. 3). The macrostructure is determined by the
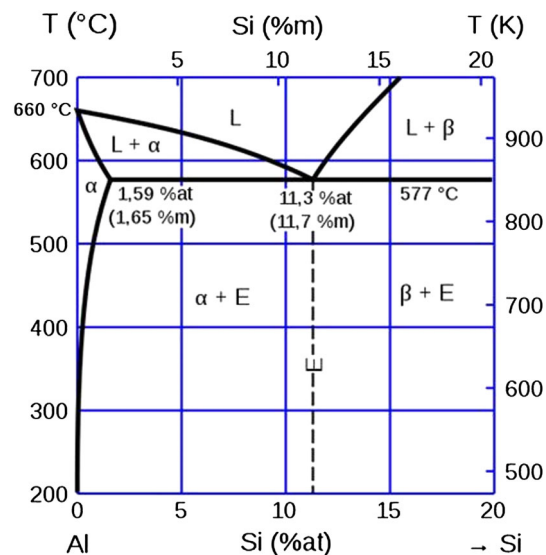

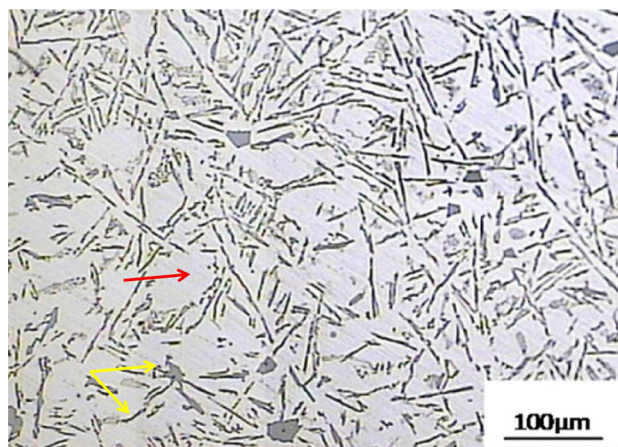**Fig. 1** Eutectic region of an Al–Si phase diagram (Makhlouf and Guthy [6])

Fig. 2 Typical microstructure of an Al–Si cast alloy. *Red arrow* marks the Al matrix; *Yellow arrows* mark the Si particles in the eutectic mixture [7]

way in which the different individual melt pools are combined. In other words, it is defined by the method of scanning the product's cross section and is also known as the building strategy of the component. In Fig. 3(a) and (b), two cross-sectional views are shown: top and front views. It is shown that the solidified melt pools are approximately half-cylindrical in shape, and the approximate size can be determined based on the cross section of the front view. The melt pool height was determined to be about 150 μm and the width to be about 300 μm (Fig. 4). The applied hatch spacing of 200 μm causes an overlap of about 33% of the melt pool width between neighboring scan tracks. Due to the half-cylindrical shape of the melt pool and the
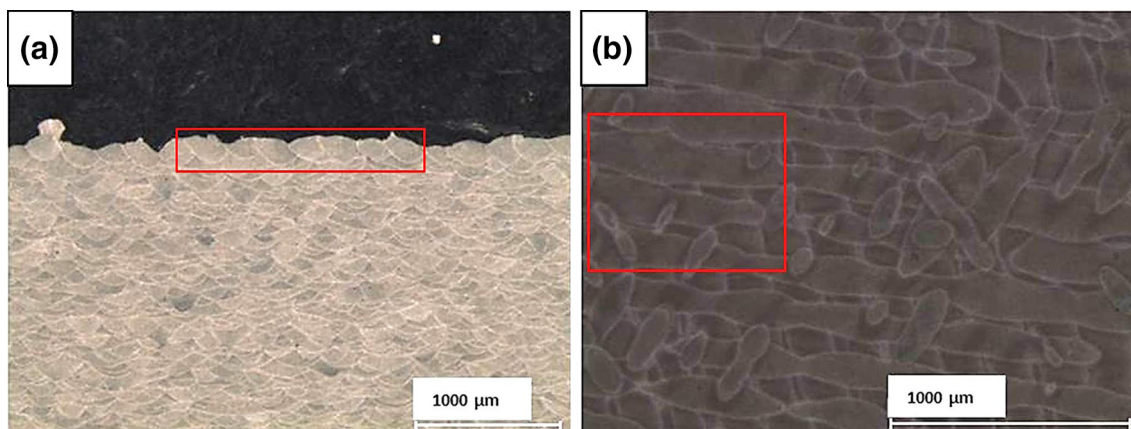
Fig. 3 Macrostructure of the specimens, examples for track segments are marked in *red*: (**a**) front view showing the "fish scale" morphology with melt pool overlapping; (**b**) top view showing variation of shape and discontinuity of the melt pools produced in different layers

Fig. 4 Close up of track segments, showing the dimensions of the half-cylindrical melt pools. Early formation of a defect can be seen marked by the *arrow*

partial remelting of formerly deposited layers, the cross section of melt pools from different layers can be observed in the top view. Due to the variations in depth and shape of the melt pools, they are not always continuous; melt pools produced in up to four different layers are marked in Fig. 3(b).

The microstructure of the components fabricated by the AM method is the end result of pre-alloyed powder melting/solidification, while the adjacent neighboring tracks cause partial remelting of the solidified tracks. During the build process, each initial seam was remelted locally up to four times, ensuring chemical homogeneity and microstructural regularity of the final structure. The combined effect of directional cooling and rapid solidification induced by repeated thermal cycles has a profound influence on the microstructures of the alloy deposited as explained in the previous paragraph. The microstructure of

Table 1 Properties of the specimens fabricated in the vertical build direction

Young modulus, GPa	Yield stress, MPa	UTS, MPa	Elongation at UTS, %
70.3	170	272	7.8
70.1	170	277	8.7
69.5	168	273	8.2
73.0	167	269	8.0

the AM samples differs completely from those fabricated by casting (as seen in Fig. 2). This has a direct effect on mechanical properties and is addressed in the mechanical properties section.

For both building directions, the microstructures within each layer share similarities and depend on the level of thermal gradient and its direction at the boundary of the moving fusion zone (FZ). Three main areas of different microstructures are observed in the samples (Fig. 4), namely 1-coarse FZ, 3-fine FZ cellular structure inside the melt pool, and 2-heat-affected zone (HAZ) appearing as broken cells between the FZs. The relatively narrow HAZ is attributed to the limited amount of heat from the concentrated laser beam.

The intercellular network is broken outside the FZ (area 2) by coarsening of the silicon phase into idiomorphic
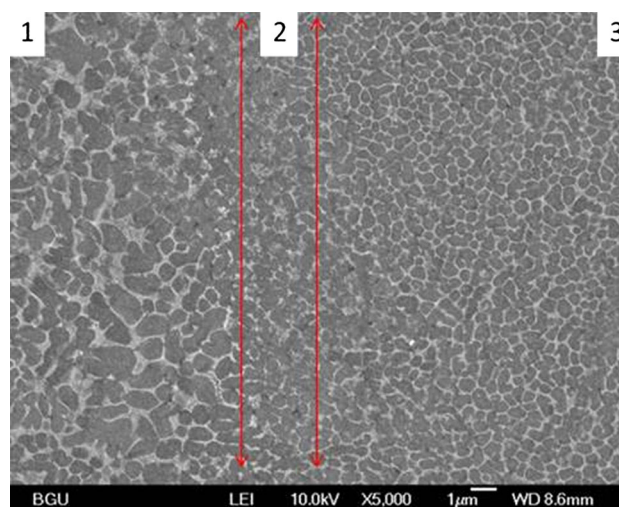

Fig. 5 Microstructures of the fusion zone; *1*—coarse fusion zone; *2*—heat-affected zone; *3*—fine fusion zone
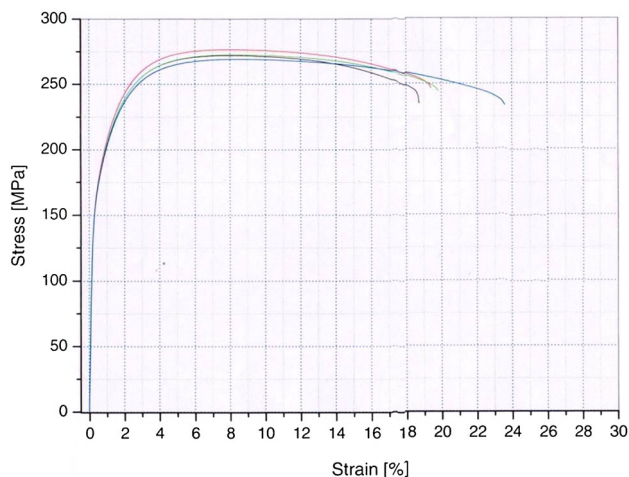
Fig. 6 Engineering stress–strain curves for the vertical build direction specimens

Table 2 Properties of the specimens fabricated in the horizontal build direction

Young's modulus, GPa	Yield stress, MPa	UTS, MPa	Elongation at UTS, %
71.3	168	267	8.6
69.0	170	267	9.5

particles, as a result of the formation of a narrow partially melted zone in the HAZ adjacent to the fusion front. The fast melting process of the stochastic powder bed can induce vigorous melt pool movements which sometimes lead to faults acting as starting points for defects such as channels and/or pores bridging between layers.

Some semi-quantitative correlations between microstructure and SLM parameters may be derived from the experimental observations and data reported in literature [2, 8, 9]. The solidification structure depends on the thermal gradient in the melt pool (G, K/m) and the growth rate (R, m/s) [8]. The growth rate (R) depends on the speed of the moving laser beam or heat source (V) and the angle between the direction of the moving source and the growth direction of the solidifying material. The G/R ratio determines the stability of the solidification front and the resulting solidification mode. For an increasing R and a constant G, the solidification can change from a stable planar solidification front, at low values of R, to cellular and finally dendrite solidification morphologies with increasing values of R. The product of G and R (K/s) gives the cooling rate, and the higher product yields a finer structure [8].

Over the course of AM-SLM, the thermal gradient and growth rate vary over the FZ. The growth rate even reaches zero at the melt pool edge, where the laser movement direction is perpendicular to the heat transfer direction.

According to Fig. 4, the morphology of the solidification structure does not change throughout the sample, while the degree of grain size does vary. This means that the G/R ratio is approximately constant and both G and R change in a similar way; however, the product of G and R varies notably.

In order to roughly estimate the R value for the AM-SLM process, we used the experimental value of cooling rate 10^6 K/s, obtained during rapid solidification of 40-μm-thick ribbons of Al-12 wt% Si [9] and the highest temperature gradient in the FZ (10^6 K/m) suggested by Thijs et al. [2]. Thus, the calculated R value is about 1000 mm/s.
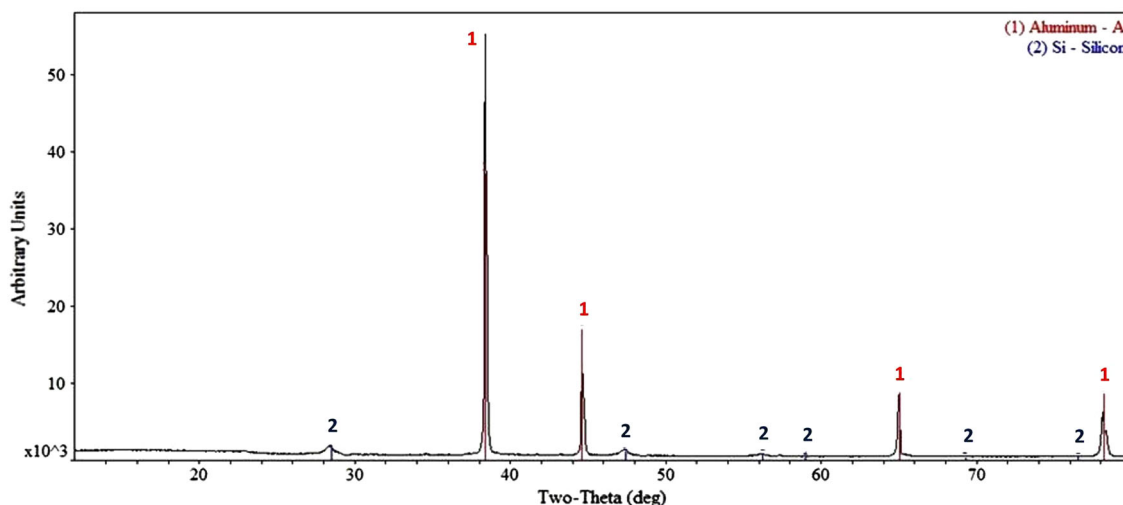

Fig. 7 XRD results for the AlSi10Mg AM-SLM processed part showing peaks in relation to the Al phase (*1*) and Si phase (*2*)
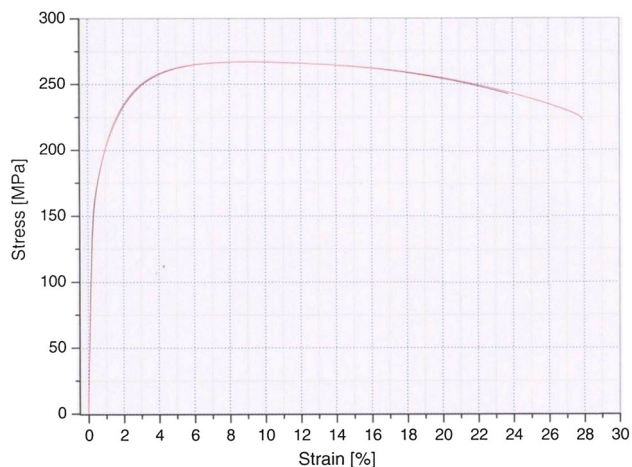
Fig. 8 Engineering stress–strain curves for the horizontal direction specimens

Fig. 10 Fracture surface of the specimen built in the horizontal direction. *Arrows* mark the "dimpled ridges"; a higher magnification is shown in the *top right corner*

This value is close to the scanning velocity of the laser beam used in this research.

Tensile Properties

Samples Fabricated in the Vertical Build Direction

The results of testing are given in Table 1 and Fig. 5.

There are no remarkable differences between mechanical properties of the heat-treated cast alloys [10, 11] and the AM samples, except for the values of elongation which are significantly higher than those reported in the literature for cast alloys after T6 treatment (3.5% elongation). The improved elongation of the AM-processed parts is attributed to the fine microstructure. Moreover, in regular Al–Si cast alloys, a strengthening mechanism is related to the formation of Mg_2Si precipitates. However, in AM parts,
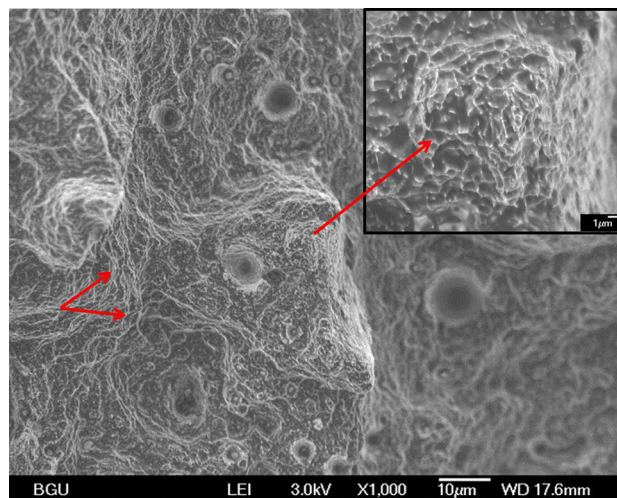
these precipitates were not detected by SEM (Fig. 4) and XRD analysis (Fig. 6). The absence of the precipitates may also lead to the increase in elongation value.

Samples Fabricated in the Horizontal Direction

The results of testing are given in Table 2 and Fig. 7.

The main difference in the properties of the specimens fabricated in horizontal direction compared with vertically built specimens is the higher values of the elongation. This reflects an expected anisotropy of AM specimens, since a directional solidification takes place during the process.

Microhardness of the AM specimens fabricated in both horizontal and vertical build directions was about 94 ± 5 HV (Fig. 8).
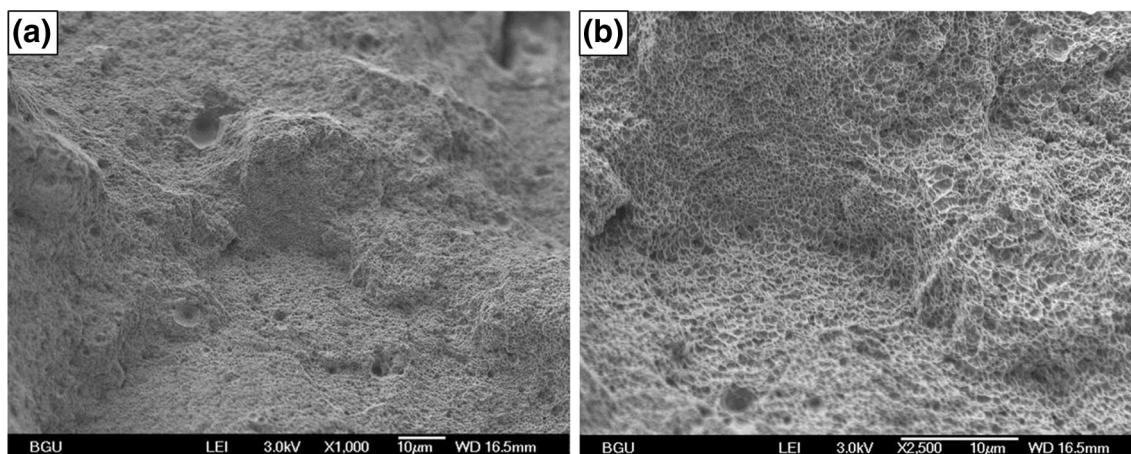

Fig. 9 Fracture surface of the specimen fabricated in the vertical build direction. (**a**) The dimpled structure between weakly bonded layers is revealed. (**b**) Higher magnification of the fine dimples

Fractography

The specimen fabricated in the vertical building direction exhibited a predominantly ductile failure (dimpled structure) located in-between weakly bonded layers (Fig. 9a). The extremely fine cellular Al–Si eutectic microstructure is discernible (Fig. 9b), and no un-melted starting powder particles were detected. Only micro-porosity (10–50 μm) was observed which can be attributed to gas entrapment (Fig. 9a).

The fracture surface of the horizontally built specimen (Fig. 10) differs completely from the vertical build direction specimens and further confirms the anisotropy attained during the AM process. This specimen displays fine dimples, without a visible cellular structure, but rather dense lines along ridges. Pores are still present in this specimen, suggesting their relation to the process. As opposed to the failure in-between weakly bonded layers of the samples fabricated in the vertical build direction, the failure of the sample fabricated in the horizontal direction occurs within each layer and provides the slightly higher elongation values (see Tables 1, 2).

Conclusions

Macro- and microstructure along with mechanical properties of the parts fabricated by AM-SLM process were investigated. The macrostructure of the product is a collage of solidified track segments, which were remelted several times by the adjacent neighboring tracks. The microstructure consists of fine cellular dendrites, which reflect high thermal gradients and rapid progression of the scanning laser during the AM process. Microstructural analysis revealed anisotropy of specimens depending on the building direction. AM-SLM processed specimens have significantly improved elongation properties in comparison to specimens fabricated by conventional casting processes. The analysis of the fracture surfaces indicates a ductile

mode of failure and the presence of the residual porosity. Further investigation has to be conducted in order to clarify the effect of processing parameters on the microstructure and the mechanical properties of products.

References

1. D. Buchbinder, H. Schleifenbaum, S. Heidrich, W. Meiners, J. Bültmann, High Power Selective Laser Melting (HP SLM) of Aluminum Parts. Phys. Proc. **12**, 271–278 (2011)
2. L. Thijs, K. Kempen, J.P. Kruth, J.V. Humbeeck, Fine-Structured Aluminium Products with Controllable Texture by Selective Laser Melting of Pre-alloyed AlSi10Mg Powder. Acta Mater. **61**, 1809–1819 (2013)
3. E. Brandl, U. Heckenberger, V. Holzinger, D. Buchbinder, Additive Manufactured AlSi10Mg Samples using Selective Laser Melting (SLM): Microstructure, High Cycle Fatigue and Fracture Behavior. Mater. Des. **34**, 159–169 (2012)
4. W.M. Steen, *Laser material processing*, 3rd edn. (Springer, Berlin, 2003), pp. 279–284
5. G.P. Dinda, A.K. Dasgupta, J. Mazumder, Evolution of microstructure in laser deposited Al–11.28%Si alloy. Surf. Coat. Technol. **206**, 2152–2160 (2012)
6. M.M. Makhlouf, H.V. Guthy, The aluminum–silicon eutectic reaction: mechanisms and crystallography. J. Light Met. **1**, 199–218 (2001)
7. R. Wang, W. Lu, Direct electrolytic Al–Si alloys (DEASA)—an undercooled alloy self-modified structure and mechanical properties, in *Electrolysis*, ed. by V. Linkov (Intech, Rijeka, 2012), pp. 107–140
8. S. Kou, *Welding Metallurgy*, 2nd edn. (Wiley, New Jersey, 2003)
9. Y. Birol, Microstructural characterization of a rapidly-solidified Al–12 wt% Si alloy. J. Mater. Sci. **31**, 2139–2143 (1996)
10. ASTM Standard B26/B26M, *Standard Specification for Aluminum-Alloy Sand Casting* (ASTM International, West Conshohocken, 2012)
11. K. Kempen, J. Thijs, J.V. Humbeeck, J.-P. Kruth, Mechanical properties of AlSi10Mg produced by selective laser melting. Phys. Proc. **39**, 439–446 (2012)